JOURNAL OF GEOPHYSICAL RESEARCH, VOL. 115, B06202, doi:10.1029/2009JB006672, 2010



# Spectral analysis of synthetic quartzofeldspathic glasses using laboratory thermal infrared spectroscopy

Rachel J. Lee,[1] Penelope L. King,[2] and Michael S. Ramsey[1]

Received 7 June 2009; revised 4 December 2009; accepted 8 January 2010; published 2 June 2010.

[1] Si-O-Si bond vibrations within silicate materials produce a prominent absorption feature in the 8–12 $\mu$m region of thermal infrared (TIR) spectra. The wavelength position of this absorption varies with $SiO_2$ content and may be used to determine rock composition. However, the presence of glass greatly affects the measurement of emitted and reflected TIR energy from the surface, a phenomenon which is not currently well understood. This study examines the TIR spectral characteristics of a suite of synthetic high-$SiO_2$ quartzofeldspathic glasses that vary systematically in composition. Glasses were synthesized in the albite-quartz, oligoclase-quartz, and andesine-quartz systems. Microreflectance (~1000 $\mu m^2$) and TIR emission spectra (bulk sample) were collected, and the spectral band maxima and minima were determined for each. Reflectance band maximum positions show a strong correlation with emissivity band minimum positions, indicating that the two types of spectra are comparable for this study. Excellent correlations are obtained between weight percent $SiO_2$ and reflectance maxima position, emission minima position, and spectral shoulder position. Molar Al/[Al+Si] and [Na+Ca]/Si are all well-correlated with reflectance maxima and shoulder positions but slightly less correlated with emission minima. Results of this study will contribute to a better understanding of spectral properties of quartzofeldspathic glasses and will provide a means to more accurately detect and map glassy surfaces (e.g., volcanoes and impact craters) remotely from the ground and from orbit.

**Citation:** Lee, R. J., P. L. King, and M. S. Ramsey (2010), Spectral analysis of synthetic quartzofeldspathic glasses using laboratory thermal infrared spectroscopy, *J. Geophys. Res.*, *115*, B06202, doi:10.1029/2009JB006672.

## 1. Introduction

[2] Thermal infrared (TIR) remote sensing and laboratory-based spectroscopy are useful tools for nondestructively analyzing planetary surfaces and small-scale samples, respectively. In the TIR wavelength range (~5–50 $\mu$m or ~2000–200 $cm^{-1}$), Si-O-Si and Si-O-Al bonds (referred to as Si-O bonds henceforth) within a silicate material undergo stretching and bending vibrations, which create absorptions at discrete wavelengths in the spectrum of the material [*King et al.*, 2004, and references therein]. Most geologic studies using emission or reflectance TIR methods have focused primarily on crystalline minerals (i.e., those which possess high-order molecular structure) that have unique and identifiable spectral features. However, amorphous and structurally disordered silicate glasses show only a very broad Reststrahlen feature in the ~1100–800 $cm^{-1}$ (~8–12 $\mu$m) region due to Si-O asymmetric stretching vibrations, and a feature between 500 and 400 $cm^{-1}$ (20–25 $\mu$m) due to bending vibrations [*Bell et al.*, 1968; *Dowty*, 1987; *Salisbury et al.*, 1991; *Poe et al.*, 1992; *McMillan and Wolf,* 1995; *Agarwal and Tomozawa*, 1997; *McMillan et al.*, 1998]. An additional spectral shoulder feature exists at ~1200 $cm^{-1}$ (~8.3 $\mu$m). These features are common to all silicate glasses regardless of composition, making them especially problematic to distinguish using TIR spectra. Furthermore, the specific wavelength location, morphology and depth of these absorptions in glassy silicate materials depend on a variety of factors, including composition, degree of crystallinity, micron-scale surface roughness, and temperature. It would be useful to better understand these complexities of TIR spectra, so that silicate glass composition may be more accurately determined.

[3] TIR data have been used extensively to derive information about silicate materials, either remotely or on the hand sample scale. For example, TIR can be used to determine silicate composition [*Salisbury et al.*, 1991; *Wyatt et al.*, 2001; *Minitti et al.*, 2002; *Wright and Ramsey*, 2006], relative age [*Kahle et al.*, 1988; *Crisp et al.*, 1990; *Realmuto et al.*, 1992], surface textures [*Ondrusek et al.*, 1993; *Ramsey and Fink*, 1999; *Byrnes et al.*, 2004; *Ramsey and Dehn*, 2004], physical properties [*Walter and Salisbury*, 1989; *Christensen et al.,* 2000], and temperature [*Vaughan et al.*, 2005; *Carter et al.*, 2007].

[1]Department of Geology and Planetary Science, University of Pittsburgh, Pittsburgh, Pennsylvania, USA.
[2]Institute of Meteoritics, University of New Mexico, Albuquerque, New Mexico, USA.


0148-0227/10/2009JB006672

[4] Natural silicate glasses can form as a result of impact-related shock metamorphism [*Johnson et al.*, 2003, 2006], alteration, and disordering of the crystal structure of a crystalline mineral or melt [*McMillan and Wolf*, 1995; *Stebbins*, 1995; *Henderson*, 2005; *Henderson et al.*, 2006]. However, they occur most commonly in volcanic environments on planetary surfaces. Active silicic domes are steep-sided masses of volatile-rich, glassy lava that may explode or collapse catastrophically, posing a potential hazard to populated areas. As they grow and collapse, these domes can undergo changes in both composition and surface texture [*Fink and Anderson*, 2000]. The study of lava dome composition and behavior is of great importance, because even subtle transitions in composition, temperature and texture can indicate an increase in the explosive potential of the dome. The energy emitted from an actively cooling dome surface is complex, with constantly varying compositions, temperatures, vesicularities, and glass percentages as the dome grows and collapses. For the purposes of volcanic hazard mitigation and assessment it is vital to understand how these petrologic properties contribute to, and affect, the emitted energy from a silicic volcanic dome.

[5] Despite their prevalence in potentially hazardous volcanic environments on Earth and their ubiquitous presence on other planetary bodies (e.g., the Moon and Mars), there have been relatively few studies that systematically examine infrared (IR) reflectance and emission spectra of glasses as a function of composition [*Sweet and White*, 1969; *Wyatt et al.*, 2001, *Byrnes et al.*, 2004, 2007; *Dalby et al.*, 2006; *Dalby and King*, 2006; *Minitti et al.*, 2006, 2007; *Dufresne et al.*, 2009]. The goal of this investigation is to expand upon the work of *Byrnes et al.* [2007], using a similar systematic experimental approach to identify and characterize distinctive spectral features in a suite of compositionally diverse synthetic high-$SiO_2$ glasses. A better understanding of how the silicate structure of glass affects spectral signatures in the TIR will improve the detection and characterization of glasses, particularly those associated with volcanic environments, and will contribute to the accuracy and mapping capabilities of TIR remote sensing on Earth and other planetary bodies.

## 2. Experimental Procedures

[6] Glasses were synthesized at the University of Western Ontario (UWO), and consist of mixtures of albite/quartz, oligoclase/quartz, and andesine/quartz, as well as albite, andesine, and oligoclase end-members. Mixtures were chosen to represent a range of compositions found in dacite/rhyolite glassy volcanic domes and flows. Each mineral was ground to a powder (~20–80 $\mu$m) in an agate mortar and pestle under ethanol, dried in a 110°C oven for several hours, and then mixed in various proportions to create the suite of glasses. For the albite-quartz glasses, $Na_2CO_3$, $SiO_2$, and $Al_2O_3$ powders were used as starting materials for albite, because most natural albites contain alteration minerals which affect their bulk composition.

[7] The starting materials were packed tightly into platinum crucibles, covered with lids, and melted in a Thermolyne box furnace for six hours. Melting temperatures varied between 1475°C and 1600°C, and were at least 200°C higher than the liquidus temperature from an Ab-An-Q phase diagram [*Schairer*, 1957]. After melting, each glass was rapidly quenched in an ice water bath, and removed from the platinum crucible. A polarized petrographic microscope was used to examine each glass for the presence of microlite crystals. If crystals were present, the glass was reground and remelted for <2 h at a slightly higher temperature.

## 3. Analytical Procedures

### 3.1. Electron Microprobe Analysis

[8] Each glass was characterized with a JEOL 8200 electron microprobe at the University of New Mexico (UNM) using a 15 kV, 5 nA, 20 $\mu$m beam, wavelength dispersive spectroscopy, and ZAF corrections. Although glass compositions could be calculated using the mineral mixture compositions, we found that the measured compositions did not precisely agree with the calculations because (1) the original minerals contained inclusions, (2) the minerals were not pure end-members, and (3) alkali loss may have occurred during synthesis. Therefore, the electron microprobe–determined compositions were used in all subsequent data analysis.

### 3.2. Microreflectance Fourier Transform Infrared Spectroscopy

[9] Microspecular reflectance measurements were collected at UWO, using a Nexus 670 FTIR spectrometer with a Continuum micro-FTIR microscope attachment. A collimated Globar source, an extended range potassium bromide (XT-KBr) beam splitter, and a mercury cadmium telluride (MCT-A) detector with a spectral range of 4000–650 $cm^{-1}$ (2.5–15.4 $\mu$m) were used. Two to three small grains of each glass (1–2 mm in size) were mounted in epoxy, and polished flat. Glasses were placed in a purged chamber in the microscope, and four individual infrared microreflectance (percent R) spectra (at 400 scans each) were collected at different locations on each glass at a resolution of 4 $cm^{-1}$. A background spectrum of a gold standard was collected prior to the glass analysis. Finally, the four spectra for each glass were averaged, and the wave number position of the percent R maximum for each was recorded. The percent R shoulder position was found by taking the second derivative of each averaged spectrum.

### 3.3. Fourier Transform Thermal Emission Spectroscopy

[10] Thermal emission spectra were collected in the Image Visualization and Infrared Spectroscopy (IVIS) Laboratory, at the University of Pittsburgh (UP). The IVIS Nexus 870 spectrometer uses a KBr beam splitter, and a deuterated triglycerine sulfate (DTGS) detector with a spectral range of 2000–400 $cm^{-1}$ (5.0–25.0 $\mu$m). Glasses were sieved into small (<125 $\mu$m), medium (<500 $\mu$m), and large (2–4 mm) size fractions. Medium and large size fractions were placed in an ultrasonic machine to remove clinging fine-grained particles, which can cause diffraction effects that change the intensity and shape of spectral features [*Lyon*, 1965;

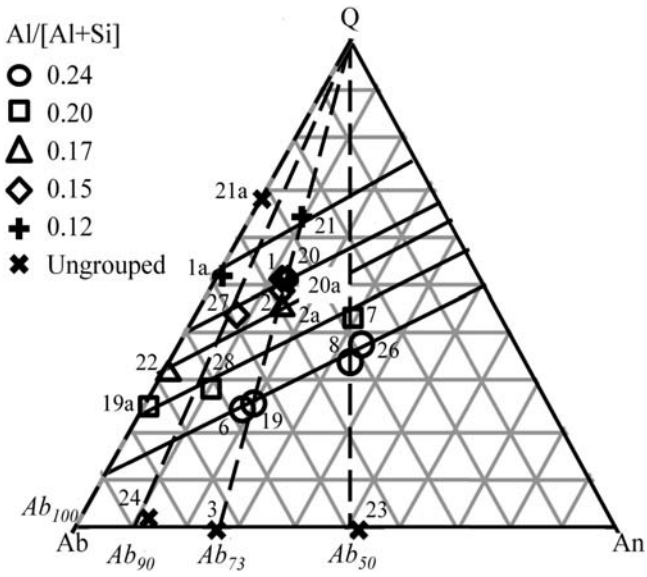


**Figure 1.** Ab-An-Q ternary diagram of the entire synthetic glass suite, from this study and from that of *Byrnes et al.* [2007]. Glass sample numbers match those listed in Table 1. Glasses are grouped by molar Al/[Al+Si] concentration. Solid lines indicate constant Al/[Al+Si]. Dashed lines denote feldspar-quartz groups (labeled in italic).

*Salisbury and Wald*, 1992; *Moersch and Christensen*, 1995; *Ramsey and Christensen*, 1998].

[11] Approximately 2 g of the medium and large size fraction of each glass were heated to 80°C for 24 h, which allowed the samples to serve as the TIR source. Prior to the glass analysis, spectra were acquired from two blackbody sources that are precision controlled to 70°C and 100°C. The spectra of the blackbody targets allow for the instrument and environmental emission to be quantified and removed [*Ruff et al.*, 1997]. Copper sample cups painted with high-emissivity paint and containing each glass were removed from the oven and placed on a heating stage within the $H_2O$ and $CO_2$ purged glove box. The temperature of the sample cups was allowed to reequilibrate prior to the collection of the spectra, which is an important factor in attaining accurate emissivity spectra [*Ramsey*, 2004]. The entire heating stage/sample cup assembly was raised into a temperature-controlled blackbody chamber that eliminated downwelling radiation. Emission spectra were collected over 250 scans, at a spectral resolution of 4 $cm^{-1}$, and averaged. Raw data were converted to absolute emissivity as described by *Ruff et al.* [1997] and the wave number position of the emissivity minimum was found for each glass spectrum. Shoulder positions were not identified for the emission spectra because they are more difficult to precisely locate on emission spectra due to the lower signal-to-noise ratio (SNR) of this technique. Furthermore, percent R and emission spectra are well correlated in this study; therefore, only the percent R shoulder positions were required.

## 4. Results

### 4.1. Glass Composition

[12] Electron microprobe data verified that the glasses were homogenous and crystal-free. Overall, the compositions were close to the intended compositions, although some glasses showed evidence of alkali loss during melting. The concentrations of albite, anorthite and quartz components were derived from the microprobe data, normalized, and plotted as individual glass compositions on an Ab-An-Q ternary diagram (Figure 1). Compositions are grouped by Al/[Al+Si] concentration because Al and Si content influences glass structure, which in turn affects spectral mor-

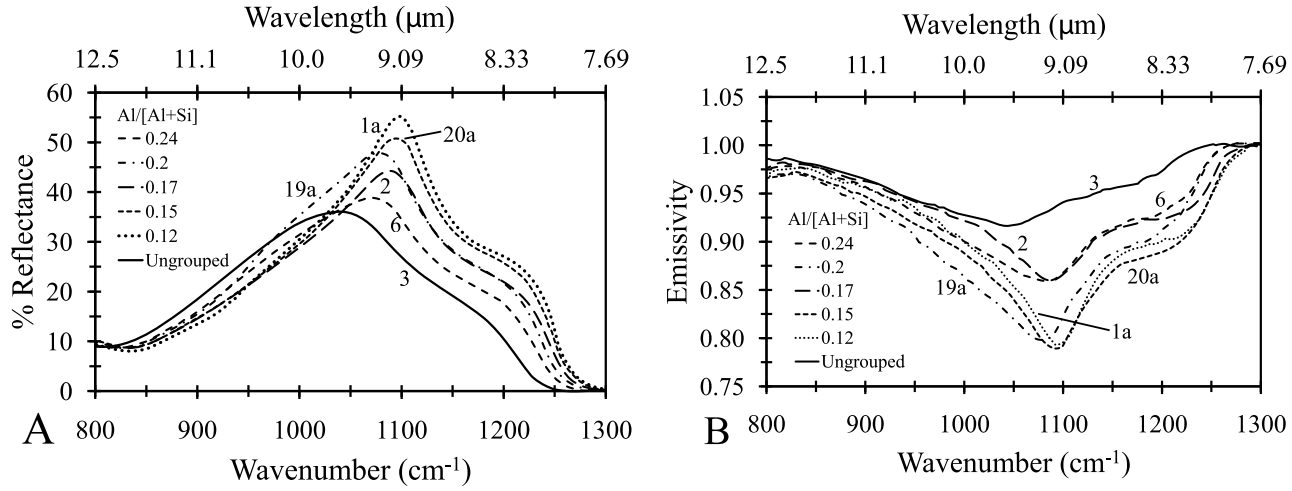


**Figure 2.** (a) Infrared microreflectance (percent R) spectra of six glasses in the compositional suite. Both the reflectance maxima (~1100 $cm^{-1}$) and the shoulders (~1200–1300 $cm^{-1}$) shift to higher wave numbers with decreasing molar Al/[Al+Si]. (b) Thermal emission spectra of the same six glasses as in Figure 2a. Emission minima (~1000–1100 $cm^{-1}$) and shoulders (~1150–1250 $cm^{-1}$) also shift to higher wave numbers with decreasing molar Al/[Al+Si].

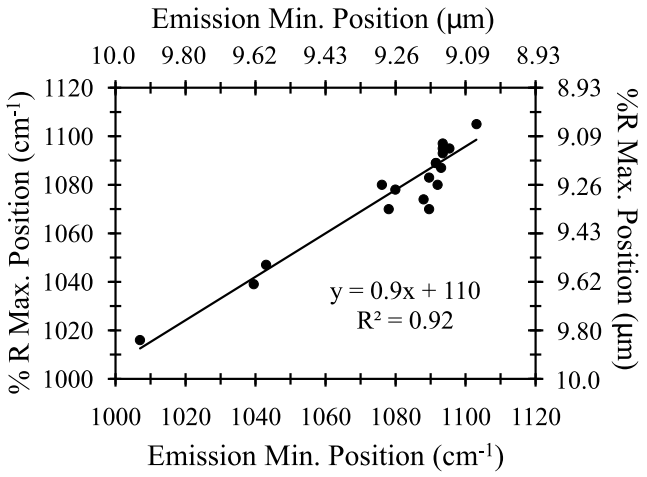


**Figure 3.** Infrared microreflectance (percent R) band maximum position versus emission band minimum position for all the samples, showing a strong degree of correlation.

phology [*Sweet and White*, 1969; *Neuville and Mysen*, 1996; *Angeli et al.*, 2000; *Dufresne et al.*, 2009].

### 4.2. Infrared Reflectance and Thermal Emission Spectra

[13] Figures 2a and 2b show percent R and thermal emission spectra, respectively, of six representative glass compositions. Each of the six glasses has a different composition, including different molar Al/[Al+Si] concentration. Both the Restsrahlen feature (~1100 $cm^{-1}$) and the ~1200 $cm^{-1}$ shoulder feature shift to higher wave numbers with increasing weight percent $SiO_2$ and decreasing molar Al/[Al+Si] content. This is consistent with previous studies involving the correlation of spectral feature position with glass composition and also holds true for silicate mineral spectra. Spectral morphology is also affected by the composition of the glass. The shoulder becomes more distinct with increasing $SiO_2$ content.

[14] The reflectance (R) spectra and emission ($\varepsilon$) spectra are generally related to each other through Kirchhoff's Law ($\varepsilon = 1 - R$) [*Nicodemus*, 1965]. Also, both spectral types show comparable changes in spectral band position and shape for the six compositions (Figures 2a and 2b). The percent R maxima positions versus emission minima positions are strongly correlated (Figure 3). Thus, for the purposes of this study, percent R spectra and thermal emission spectra are comparable.

### 4.3. Spectral Characteristics With Varying Composition

[15] Figures 4a and 4b show the wave number position of the percent R maximum and the emission minimum, respectively, versus weight percent $SiO_2$. Maxima and minima are grouped by molar Al/[Al+Si]. The percent R maxima and emission minima shift to higher wave numbers with increasing weight percent $SiO_2$, and decreasing amounts of Al. The position of the ~1200 $cm^{-1}$ shoulder in percent R spectra also increases in wave number with increasing $SiO_2$ and decreasing Al (Figure 4c).

[16] Figures 5a–5c show percent R maxima, emission minima, and percent R shoulder positions plotted against molar Al/[Al+Si]. These band locations shift to higher wave

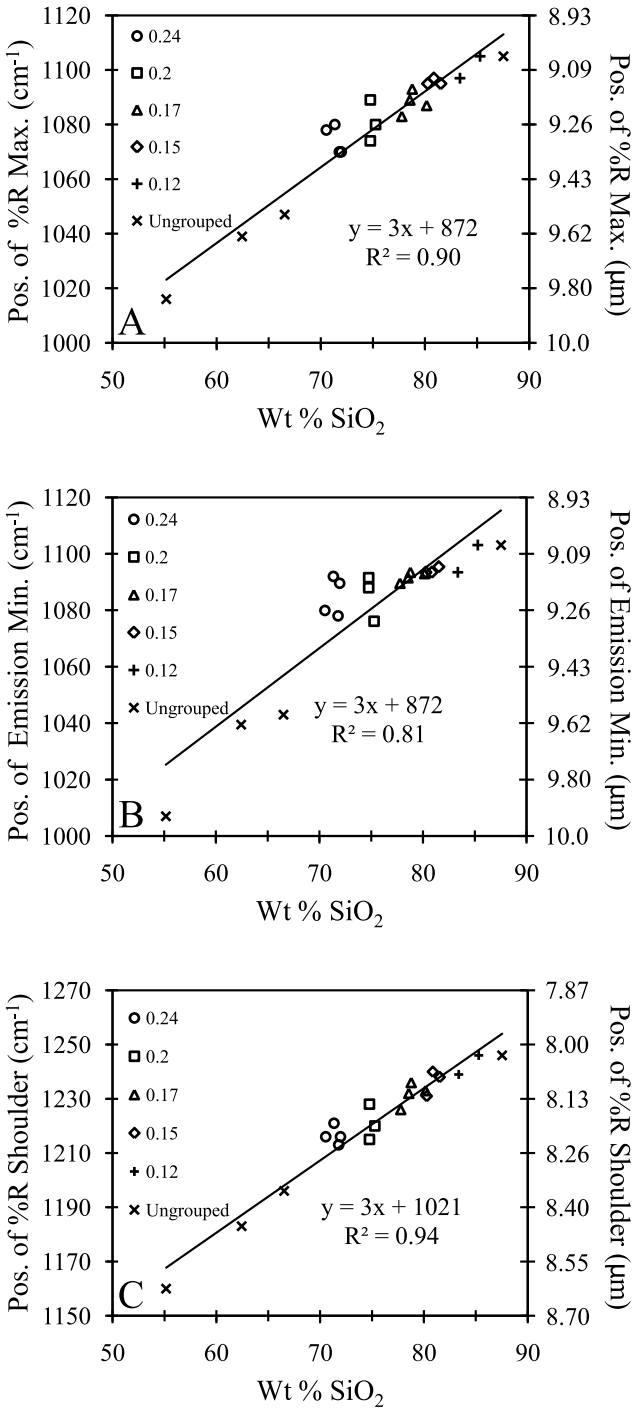


**Figure 4.** Weight percent $SiO_2$ versus (a) percent R maximum position, (b) emission minimum position, and (c) percent R shoulder position. Data are grouped by molar Al/[Al+Si] concentration. Maxima, minima, and shoulder positions increase in wave number with increasing weight percent $SiO_2$ and decreasing molar Al/[Al+Si].

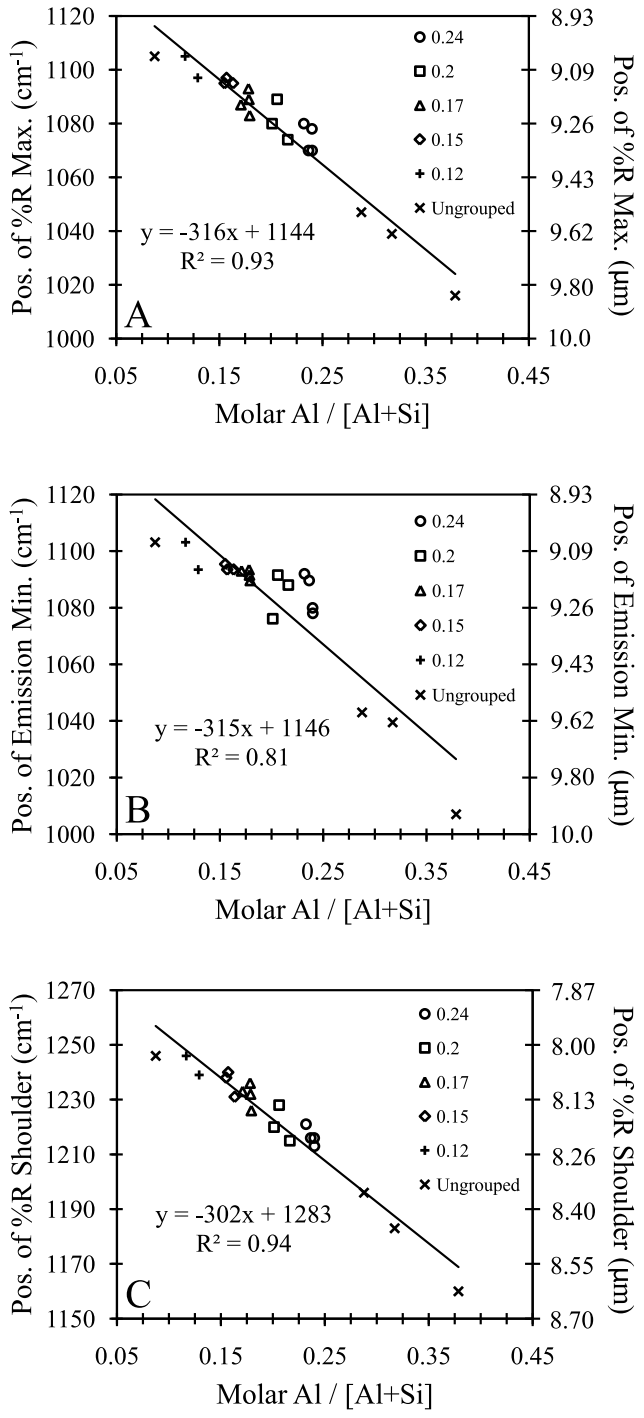


**Figure 5.** Molar Al/[Al+Si] versus (a) percent R maximum position, (b) emission minimum position, and (c) percent R shoulder position. A decrease in molar Al/[Al+Si] is associated with an increase in the maxima, minima, and shoulder positions.

numbers with decreasing molar Al/[Al+Si] content, as expected. Conversely, an increase in molar [Na+Ca]/Si in the glasses causes a shift in the percent R maxima, emission minima, and percent R shoulder positions to lower wave numbers (Figures 6a–6c). Although K is also present in most of the glasses, it was not included in the alkali analyses, because it occurs only in trace amounts (Table 1).

## 5. Discussion

### 5.1. Reflectance and Emission Spectra

[17] Kirchhoff's Law ($\varepsilon = 1 - R$) is valid only if emission spectra are directional, and reflectance spectra are either hemi-

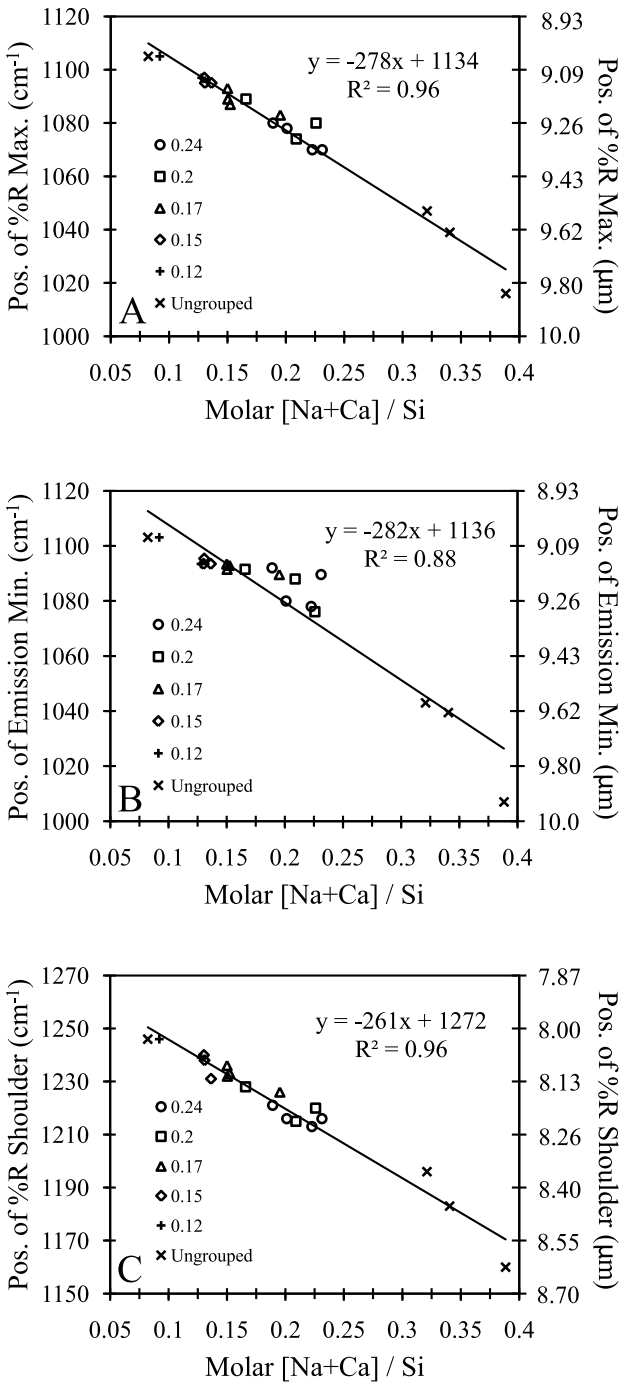


**Figure 6.** Molar [Na+Ca]/Si versus (a) percent R maximum position, (b) emission minimum position, and (c) percent R shoulder position. An increase in molar [Na+Ca]/Si causes a decrease in the maxima, minima, and shoulder positions.

**Table 1.** Compositional and Spectral Data for Glasses

| Symbol[a] | Glass | Starting Group | Ab (wt %) | An (wt %) | Q (wt %) | $SiO_2$ (wt %) | Si (mol) | Al (mol) | Na (mol) | Ca (mol) | K (mol) | Percent R Maximum ($cm^{-1}$) | Emission Minima ($cm^{-1}$) | Percent R Shoulder ($cm^{-1}$) |
|---|---|---|---|---|---|---|---|---|---|---|---|---|---|---|
| Square | 19a | Ab100 – Q | 75.31 | 0.10 | 24.60 | 75.27 | 1.25 | 0.32 | 0.28 | 0.00 | 0.00 | 1080 | 1076 | 1220 |
| Triangle | 22 | Ab100 – Q | 67.35 | 0.04 | 32.61 | 77.77 | 1.29 | 0.28 | 0.25 | 0.00 | 0.00 | 1083 | 1090 | 1226 |
| Plus | 1a | Ab100 – Q | 47.52 | 0.03 | 52.45 | 83.36 | 1.39 | 0.21 | 0.18 | 0.00 | 0.00 | 1097 | 1093 | 1239 |
| Cross | 21a | Ab100 – Q | 32.21 | 0.05 | 67.74 | 87.54 | 1.46 | 0.14 | 0.12 | 0.00 | 0.00 | 1105 | 1103 | 1246 |
| Cross | 24[b] | Ab90An10 – Q | 86.11 | 11.38 | 2.50 | 66.53 | 1.11 | 0.45 | 0.32 | 0.04 | 0.01 | 1047 | 1043 | 1196 |
| Square | 28[b] | Ab90An10 – Q | 61.37 | 9.54 | 29.09 | 74.76 | 1.24 | 0.34 | 0.23 | 0.03 | 0.01 | 1074 | 1088 | 1215 |
| Triangle | 27[b] | Ab90An10 – Q | 48.65 | 6.72 | 44.64 | 80.17 | 1.33 | 0.28 | 0.18 | 0.02 | 0.01 | 1087 | 1093 | 1233 |
| Cross | 3 | Ab73An27 – Q | 74.03 | 25.97 | 0.00 | 62.44 | 1.04 | 0.48 | 0.27 | 0.09 | 0.02 | 1039 | 1039 | 1183 |
| Circle | 6 | Ab73An27 – Q | 58.03 | 17.64 | 24.33 | 71.96 | 1.20 | 0.37 | 0.22 | 0.06 | 0.01 | 1070 | 1090 | 1216 |
| Circle | 19 | Ab73An27 – Q | 54.88 | 19.37 | 25.75 | 71.79 | 1.19 | 0.38 | 0.20 | 0.07 | 0.02 | 1070 | 1078 | 1213 |
| Triangle | 2 | Ab73An27 – Q | 40.23 | 14.21 | 45.57 | 78.78 | 1.31 | 0.28 | 0.15 | 0.05 | 0.01 | 1093 | 1093 | 1236 |
| Triangle | 2a | Ab73An27 – Q | 40.04 | 14.48 | 45.48 | 78.55 | 1.31 | 0.28 | 0.15 | 0.05 | 0.01 | 1089 | 1092 | 1232 |
| Diamond | 20a | Ab73An27 – Q | 37.04 | 13.22 | 49.74 | 80.27 | 1.34 | 0.26 | 0.14 | 0.05 | 0.01 | 1095 | 1093 | 1231 |
| Diamond | 20 | Ab73An27 – Q | 36.40 | 12.21 | 51.38 | 81.52 | 1.36 | 0.25 | 0.13 | 0.04 | 0.01 | 1095 | 1095 | 1238 |
| Diamond | 1 | Ab73An27 – Q | 36.01 | 12.41 | 51.58 | 80.85 | 1.35 | 0.25 | 0.13 | 0.04 | 0.01 | 1097 | 1093 | 1240 |
| Plus | 21 | Ab73An27 – Q | 26.28 | 9.62 | 64.11 | 85.29 | 1.42 | 0.19 | 0.10 | 0.03 | 0.01 | 1105 | 1103 | 1246 |
| Cross | 23[b] | Ab50 – Q | 48.63 | 51.37 | 0.00 | 55.16 | 0.92 | 0.10 | 0.18 | 0.18 | 0.01 | 1016 | 1007 | 1160 |
| Circle | 8 | Ab50 – Q | 32.27 | 33.23 | 34.50 | 70.53 | 1.17 | 0.37 | 0.12 | 0.12 | 0.01 | 1078 | 1080 | 1216 |
| Circle | 26[b] | Ab50 – Q | 28.93 | 33.38 | 37.69 | 71.34 | 1.19 | 0.36 | 0.11 | 0.12 | 0.01 | 1080 | 1092 | 1221 |
| Square | 7 | Ab50 – Q | 28.11 | 28.69 | 43.21 | 74.75 | 1.24 | 0.32 | 0.11 | 0.10 | 0.01 | 1089 | 1092 | 1228 |

[a]Symbols represent those in Figure 1.
[b]From *Byrnes et al.* [2007].

spherical-directional or directional-hemispherical [*Hapke*, 1993; *Korb et al.*, 1999]. For this study, specular microreflectance measurements were acquired. However, glasses are amorphous and single polished glass grains were analyzed; thus, the diffusely scattered component from each sample is considered negligible and Kirchhoff's Law remains valid. In contrast, emission spectra of numerous large glass particles per sample were acquired. This results in spectra with slightly shallowed and more muted spectral features relative to the reflectance spectra, because multiple emission and reflection events between each of the particles have the effect of adding a reflected component to the spectra [*Ramsey and Fink*, 1999]. Despite the differences between emissivity spectra and reflectance spectra, a strong correlation still exists between the band shape, minima, and maxima positions. The spectra acquired from each technique are therefore directly comparable to one another.

[18] A Kramers-Kronig (KK) transform is commonly performed on reflectance spectra in order to remove optical constant effects [*McMillan and Hoffmeister*, 1988] and to compare spectral features with compositional parameters [e.g., *Sweet and White*, 1969; *Dufresne et al.*, 2009]. However, KK transforms were not applied to the reflectance spectra in this study, because the transformed data would no longer be equivalent to thermal emission spectra.

### 5.2. Compositional Controls on TIR Spectral Features

[19] Silicate glasses are made of oxygens bonded to (1) cations that form the glass network (T; fourfold network formers like $^{[4]}Si^{4+}$, $^{[4]}Al^{3+}$ and $^{[4]}Ti^{4+}$), (2) network modifiers (M; e.g., $Na^{+}$, $K^{+}$, $Mg^{2+}$ and $Ca^{2+}$) that break up the silicate network, and (3) charge compensators (e.g., $Na^{+}$, $K^{+}$ and $Ca^{2+}$) that compensate for charge deficiencies (e.g., excess $Al^{3+}$ relative to $Si^{4+}$ in aluminosilicate glasses) [e.g., *Neuville et al.*, 2004]. The network formers bond to either bridging oxygens that are bound to another network former (T-O-T bonds) or nonbridging oxygens where there is a network modifier (T-O-M bonds).

#### 5.2.1. Effect of $SiO_2$ on TIR Spectral Features

[20] Our results showing that the percent R maximum and emission minimum band locations increase as $SiO_2$ increases (Figures 4a and 4b) agree with other studies [e.g., *Sweet and White*, 1969; *Domine and Piriou*, 1983; *Poe et al.*, 1992; *McMillan et al.*, 1998; *Angeli et al.*, 2000; *De Maeyer et al.*, 2002; *Dufresne et al.,* 2009]. These studies showed that the IR peak location is related to the average bond length of the bulk glass: as $SiO_2$ increases, the average bond in the glass is shorter. The average bond distance decreases because there is an increase in the number of T-O bonds (more polymerized) that have a shorter bond distance (~1.6–1.7 Å) relative to M-O bonds (less polymerized) that have longer bond distances (~2–3 Å) and higher coordination numbers [e.g., *De Maeyer et al.*, 2002; *Guillot and Sator*, 2007].

[21] Similarly, the position of the percent R shoulder location increases as $SiO_2$ increases (Figure 4c). This observation is consistent with previous workers [e.g., *Dalby et al.*, 2006; *King et al.*, 2008; *Dufresne et al.*, 2009]. Because the position of the percent R shoulder location is highly correlated with weight percent $SiO_2$ ($R^2 = 0.94$) with little scatter (Figure 4c) it is probable that the average bonds contributing to this vibrational feature are highly polymerized, shorter bonds (e.g., like those in $SiO_2$ glass).

#### 5.2.2. Effect of Molar Al/[Al+Si] and [Na+Ca]/Si on TIR Spectral Features

[22] If the local charge balance is disrupted (e.g., by adding excess $Na^{+}$, $K^{+}$, or $Ca^{2+}$), then Al may become a network modifier with either fivefold or sixfold coordination ($^{[5]}Al$ or $^{[6]}Al$). The influence of Al coordination, Al content, alkali and alkaline earth content on glass structure have all been extensively examined using Raman spectroscopy [e.g., *Neuville and Mysen*, 1996; *Neuville et al.*, 2004, 2006].

Those studies found that the addition of $^{[4]}$Al to silicate glasses results in Raman silicate stretching bands at 900–1300 $cm^{-1}$ that show a progressive decrease to lower wave numbers. However, this spectral effect is not observed with $^{[5]}$Al or $^{[6]}$Al.

[23] Our study examined the effect of adding $^{[4]}$Al because we added Al by adding feldspars, without adding excess charge. We find that the addition of $^{[4]}$Al, examined in terms of molar Al/[Al+Si], causes the Si-O band position to shift to lower wave numbers in percent R spectra (Figures 5a and 5c) and emission spectra (Figure 5b). Our findings are supported by observations in other glasses, where increasing Al/[Al+Si] results in longer average bond distances (e.g., alkali aluminosilicate glasses [*Neuville and Mysen*, 1996]).

[24] Because alkali and alkaline earth oxides strongly affect glass structure and bond lengths, we also examined the effect on spectral features of adding molar [Na+Ca] relative to Si (i.e., increasing molar [Na+Ca]/Si, but charge balancing with $^{[4]}Al^{3+}$). Due to the large effect of Si, increasing molar [Na+Ca]/Si causes the Si-O band positions to decrease in wave number and intensity, and broaden, as the Si-O bond angle decreases and the average bond length decreases [e.g., *Sweet and White*, 1969; *McMillan et al.*, 1998; *De Maeyer et al.*, 2002] (Figures 6a–6c). In general, the correlations between the percent R spectral features and molar [Na+Ca]/Si are excellent (i.e., high $R^2$ and little scatter).

[25] We hypothesize that Na+Ca have a stronger control on the average bond length of the glass than Al. Support for this hypothesis comes from calculations for rhyolitic glasses where $^{[8]}$Na–O bond distances are ~2.5 Å and $^{[7]}$Ca-O bond distances are ~2.4 Å; whereas, $^{[4]}$Si–O bond distances are ~1.6 Å and $^{[4]}$Al–O bond distances are ~1.7 Å [*Guillot and Sator*, 2007]. In other words, one mole of Na+Ca will have a greater effect than one mole of Al on increasing the average bond length of a silicate glass. Therefore, the factor Na+Ca/Si shows an excellent correlation with the TIR spectra because increasing Na+Ca tends to increase the average bond length and increasing Si tends to decrease the average bond length. In sum, Na+Ca/Si is a good proxy for the average bond length of these felsic glasses and therefore there is an excellent correlation between Na+Ca/Si and TIR spectral features.

### 5.3. Comparison of Spectra at Atmospheric Pressure With Spectra at High Pressure

[26] The glasses in this study were prepared at atmospheric pressure; however, felsic silicate glasses commonly form at high pressure in impact events, particularly in extraterrestrial environments. Laboratory modeling of pressure shocked plagioclase feldspars [*Johnson et al.*, 2003] and the study of shocked feldspars using thermal emission spectrometer (TES) data from Mars [*Johnson et al.*, 2006] have shown that plagioclase undergoes structural changes with increasing pressures, which affect the position and morphology of spectral features. Compression of the silica tetrahedral structure causes the average bond length (and perhaps angle) to decrease, affecting the bending and stretching motions. Spectral features thus become more muted and band depths decrease. The plagioclase Reststrahlen feature also coalesces into a single broad band near 9 $\mu$m, making the spectra more glass-like. The features of the glass spectra in the work by *Johnson et al.* [2003, 2006] shift to lower wave numbers with increasing Al content and the average bond distances increases. These findings are consistent with the data presented here, and further validate spectral features as accurate indicators of composition and structure in silicate glasses.

## 6. Conclusions

[27] The results of this study show that the general spectral morphology and the individual positions of the reflectance maxima and emission minima ($cm^{-1}$) are highly dependent on glass composition. Both reflectance maxima and emission minima show a systematic shift to higher wave number with increasing weight percent $SiO_2$ and decreasing molar Al/[Al+Si] and [Na+Ca]/Si within the glass. These observations are consistent with previous glass compositional studies and with average bond lengths of glasses. This study expands upon the suite of high-$SiO_2$ glass compositions presented by *Byrnes et al.* [2007], and further validates the thermal emission spectroscopy technique through comparison to other analytical techniques. The findings presented here may be applied to future TIR remote sensing measurements of surfaces containing a glass fraction. For example, if the spectral shape is consistent with that of glass and the wave number position is determined, then the weight percent $SiO_2$ and molar [Na+Ca]/Si could be determined.

[28] The glass suite presented here provides further insight into the behavior of silicate glass spectra in relation to composition and structure. However, the focus of this study is on laboratory-scale glasses of synthetic compositions. The study of natural glasses using remote sensing techniques introduces a number of variables that were not constrained in the laboratory study. For example, natural glasses are often glass/crystal mixes, and are commonly vesicular. Although the data in this study cannot be directly applied to remote sensing of volcanoes, it does validate thermal emission as a technique for studying glass composition.

[29] This work is the initial facet of a study that will examine the effects of short to medium-range Si-O bonding on the infrared spectra of synthetic and natural high-$SiO_2$ glasses. Future work includes the detailed compositional and spectral analysis of naturally occurring rhyolite and dacite glasses, and the implementation of a microfurnace for in situ laboratory emission experiments of synthetic and natural glasses at high temperatures and various physical states. We expect to gain a better understanding of how the silicate structure of glass directly affects TIR emission during melting and cooling through the glass transition temperature. That work, combined with these results, will help improve our ability to accurately detect and verify all volcanic glass compositions and physical states, especially during active lava emplacement. It will also contribute to the accuracy and mapping capabilities of future TIR remote sensing instruments.

[30] **Acknowledgments.** Two anonymous reviewers and Richard Arculus are thanked for their helpful comments on the manuscript. Funding for this research was made possible through a grant to M.S.R. from the Petrology and Geochemistry Program of the National Science Foundation (grant EAR-0711056) and funds to P.L.K. are from a NASA Earmark to the Institute of Meteoritics at UNM, the Canadian Foundation for Innova-

tion, and Ontario Premier's Excellence Award at UWO. Mike Spilde is thanked for help with the electron microprobe analysis.

## References


Agarwal, A., and M. Tomozawa (1997), Correlation of silica glass properties with the infrared spectra, *J. Non-Cryst. Solids*, *209*, 166–174, doi:10.1016/S0022-3093(96)00542-X.

Angeli, F., J.-M. Delaye, T. Charpentier, J.-C. Petit, D. Ghaleb, and P. Faucon (2000), Influence of glass chemical composition on the Na-O bond distance: A $^{23}$Na 3Q-MAS NMR and molecular dynamics study, *J. Non-Cryst. Solids*, *276*, 132–144, doi:10.1016/S0022-3093(00)00259-3.

Bell, R. J., N. F. Bird, and P. Dean (1968), The vibrational spectra of vitreous silica, germania, and beryllium fluoride, *J. Phys. Chem. C*, *1*, 299–303, doi:10.1088/0022-3719/1/2/304.

Byrnes, J. M., M. S. Ramsey, and D. A. Crown (2004), Surface unit characterization of the Mauna Ulu flow field, Kilauea Volcano, Hawaii, using integrated field and remote sensing analyses, *J. Volcanol. Geotherm. Res.*, *135*, 169–193, doi:10.1016/j.jvolgeores.2003.12.016.

Byrnes, J. M., P. L. King, M. S. Ramsey, and R. J. Lee (2005), Synthesis and analysis of silicate glasses: Applications to remote sensing of volcanic surface units on Earth and Mars, *Lunar Planet. Sci.* [CD-ROM], *XXXVI*, Abstract 2089.

Byrnes, J. M., P. L. King, M. S. Ramsey, and R. J. Lee (2007), Thermal infrared reflectance and emission spectroscopy of quartzofeldspathic glasses, *Geophys. Res. Lett.*, *34*, L01306, doi:10.1029/2006GL027893.

Carter, A. J., M. S. Ramsey, and A. B. Belousov (2007), Recent crater formation at Bezymianny Volcano lava dome: Significant changes observed in satellite and field data, *Bull. Volcanol.*, *69*, 811–815, doi:10.1007/s00445-007-0113-x.

Christensen, P. R., J. L. Bandfield, M. D. Smith, V. E. Hamilton, and R. N. Clark (2000), Identification of a basaltic component on the Martian surface from Thermal Emission Spectrometer data, *J. Geophys. Res.*, *105*, 9609–9621, doi:10.1029/1999JE001127.

Clark, R. N. (1999), Spectroscopy of rocks and minerals, and principles of spectroscopy, in *Manual of Remote Sensing*, vol. 3, *Remote Sensing for the Earth Sciences*, edited by A. N. Rencz, pp. 3–58, John Wiley, New York.

Crisp, J., A. B. Kahle, and E. A. Abbott (1990), Thermal infrared spectral character of Hawaiian basaltic glasses, *J. Geophys. Res.*, *95*, 21,657–21,669, doi:10.1029/JB095iB13p21657.

Dalby, K. N., and P. L. King (2006), A new approach to determine and quantify structural units in silicate glasses using micro Fourier-Transform Infrared spectroscopy, *Am. Mineral.*, *91*, 1783–1793, doi:10.2138/am.2006.2075.

Dalby, K. N., C. D. M. Dufresne, P. L. King, J. M. Byrnes, R. J. Lee, and M. S. Ramsey (2006), Characterization of glasses using infrared spectroscopy, *Geochim. Cosmochim. Acta*, *70*(18), Suppl.1, A125, doi:10.1016/j.gca.2006.06.267.

De Maeyer, E. A. P., R. M. H. Verbeeck, and C. W. J. Vercruysse (2002), Infrared spectrometric study of acid-degradable glasses, *J. Dent. Res.*, *81*, 552–555, doi:10.1177/154405910208100810.

Domine, F., and B. Piriou (1983), Study of sodium silicate melt and glass by infrared reflectance spectroscopy, *J. Non-Cryst. Solids*, *55*, 125–130, doi:10.1016/0022-3093(83)90012-1.

Dowty, E. (1987), Vibrational interactions of tetrahedral in silicate glasses and crystals: 1. Calculations on ideal silicate-aluminate-germanate structural units, *Phys. Chem. Miner.*, *14*, 80–93, doi:10.1007/BF00311151.

Dufresne, C. D. M., P. L. King, M. Darby Dyar, and K. N. Dalby (2009), Effect of $SiO_2$, total FeO, $Fe^{3+}/Fe^{2+}$, and alkali elements in basaltic glasses on mid-infrared spectra, *Am. Mineral.*, *94*(11–12), 1580–1590, doi:10.2138/am.2009.3113.

Fink, J. H., and S. W. Anderson (2000), Lava domes and coulees, in *Encyclopedia of Volcanoes*, edited by H. Sigurdsson et al., pp. 307–319, Academic, San Diego, Calif.

Guillot, B., and N. Sator (2007), A computer simulation study of natural silicate melts. Part I: Low pressure properties, *Geochim. Cosmochim. Acta*, *71*, 1249–1265, doi:10.1016/j.gca.2006.11.015.

Hapke, B. (1993), *Theory of Reflectance and Emittance Spectroscopy*, 455 pp., Cambridge Univ. Press, New York, doi:10.1017/CBO9780511524998.

Henderson, G. S. (2005), The structure of silicate melts: A glass perspective, *Can. Mineral.*, *43*, 1921–1958, doi:10.2113/gscanmin.43.6.1921.

Henderson, G. S., G. Calas, and J. F. Stebbins (2006), The structure of silicate glasses and melts, *Elements*, *2*, 269–273, doi:10.2113/gselements.2.5.269.

Johnson, J. R., F. Horz, and M. I. Staid (2003), Thermal infrared spectroscopy and modeling of experimentally shocked plagioclase feldspars, *Am. Mineral.*, *88*, 1575–1582.

Johnson, J. R., M. I. Staid, T. N. Titus, and K. Becker (2006), Shocked plagioclase signatures in Thermal Emission Spectrometer data of Mars, *Icarus*, *180*(1), 60–74, doi:10.1016/j.icarus.2005.08.010.

Kahle, A. B., A. R. Gillespie, E. A. Abbott, M. J. Abrams, R. E. Walker, G. Hoover, and J. P. Lockwood (1988), Relative dating of Hawaiian lava flows using multispectral thermal infrared images: A new tool for geologic mapping of young volcanic terranes, *J. Geophys. Res.*, *93*, 15,239–15,251, doi:10.1029/JB093iB12p15239.

King, P. L., M. S. Ramsey, P. F. McMillan, and G. Swayze (2004), Laboratory Fourier transform infrared spectroscopy methods for geologic samples, in *Infrared Spectroscopy in Geochemistry, Exploration Geochemistry, and Remote Sensing*, edited by P. L. King et al., *Short Course Ser. Mineral. Assoc. Can.*, 33, 57–91.

King, P. L., C. D. M. Dufresne, and K. N. Dalby (2008), Effect of $SiO_2$, total FeO, $Fe^{2+}/Fe^{3+}$ and alkalis in glasses on thermal infrared spectra, *Lunar Planet. Sci.* [CD ROM], *XXXIX*, abstract 2256.

Korb, A. R., J. W. Salisbury, and D. M. D'Aria (1999), Thermal-infrared remote sensing and Kirchhoff's law: 2. Field measurements, *J. Geophys. Res.*, *104*, 15,339–15,350, doi:10.1029/97JB03537.

Lyon, R. J. P. (1965), Analysis of rocks by spectral infrared emission (8 to 25 microns), *Econ. Geol.*, *60*, 715–736, doi:10.2113/gsecongeo.60.4.715.

McMillan, P. F., and A. Hoffmeister (1988), Infrared and Raman spectroscopy, in *Spectroscopic Methods in Mineralogy and Geology*, edited by F. C. Hawthorne, *Rev. Mineral.*, vol. 18, PP. 99–159, Mineral. Soc. of Am., Reston, Va.

McMillan, P. F., and G. H. Wolf (1995), Vibrational spectroscopy of silicate liquids, in *Structure, Dynamics and Properties of Silicate Melts*, *Rev. Mineral.*, vol. 33, edited by J. F. Stebbins et al., pp. 247–315, Mineral. Soc. of Am., Blacksburg, Va.

McMillan, P. F., A. Grzechnik, and H. Chotalla (1998), Structural characterization of $SiO_2$±$CsAlO_2$ and $SiO_2$±$RbAlO_2$ glasses, *J. Non-Cryst. Solids*, *226*, 239–248, doi:10.1016/S0022-3093(98)00416-5.

Minitti, M. E., J. F. Mustard, and M. J. Rutherford (2002), Effects of glass content and oxidation on the spectra of SNC-like basalts: Applications to Mars remote sensing, *J. Geophys. Res.*, *107*(E5), 5030, doi:10.1029/2001JE001518.

Minitti, M. E., M. B. Wyatt, and V. E. Hamilton (2006), Investigating the role of compositionally diverse glasses in interpreting Martian chemistry and mineralogy as viewed by TES, *Eos Trans. AGU*, *87*(52), Fall Meet. Suppl., Abstract P23C-0067.

Minitti, M. E., C. M. Weitz, M. D. Lane, and J. L. Bishop (2007), Morphology, chemistry, and spectral properties of Hawaiian rock coatings and implications for Mars, *J. Geophys. Res.*, *112*, E05015, doi:10.1029/2006JE002839.

Moersch, J. E., and P. R. Christensen (1995), Thermal emission from particulate surfaces: A comparison of scattering models with measured spectra, *J. Geophys. Res.*, *100*, 7465–7477, doi:10.1029/94JE03330.

Neuville, D. R., and B. O. Mysen (1996), Role of aluminum in the silicate network: In situ, high-temperature study of glasses and melts on the join $SiO_2$-$NaAlO_2$, *Geochim. Cosmochim. Acta*, *60*, 1727–1737, doi:10.1016/0016-7037(96)00049-X.

Neuville, D. R., L. Cormier, and D. Massiot (2004), Al environment in tectosilicate and peraluminous glasses: A 27Al MQ-MAS NMR, Raman, and XANES investigation, *Geochim. Cosmochim. Acta*, *68*, 5071–5079, doi:10.1016/j.gca.2004.05.048.

Neuville, D. R., L. Cormier, and D. Massiot (2006), Al coordination and speciation in calcium aluminosilicate glasses: Effects of composition determined by 27 Al MQ-MAS NMR and Raman spectroscopy, *Chem. Geol.*, *229*, 173–185, doi:10.1016/j.chemgeo.2006.01.019.

Nicodemus, F. E. (1965), Directional reflectance and emissivity of an opaque surface, *Appl. Opt.*, *4*, 767–773, doi:10.1364/AO.4.000767.

Ondrusek, J., P. R. Christensen, and J. H. Fink (1993), Mapping the distribution of vesicular textures on silicic lavas using the Thermal Infrared Multispectral Scanner, *J. Geophys. Res.*, *98*, 15,903–15,908, doi:10.1029/93JB01559.

Poe, B. T., P. F. McMillan, C. A. Angell, and R. K. Sato (1992), Al and Si coordination in $SiO_2$-$Al_2O_3$ glasses and liquids: A study by NMR and IR spectroscopy and MD simulations, *Chem. Geol.*, *96*, 333–349, doi:10.1016/0009-2541(92)90063-B.

Ramsey, M. S. (2004), Quantitative geological surface processes extracted from infrared spectroscopy and remote sensing, in *Infrared Spectroscopy in Geochemistry, Exploration Geochemistry, and Remote Sensing*, edited by P. L. King et al., *Short Course Ser. Mineral. Assoc. Can.*, *33*, 197–213.

Ramsey, M. S., and P. R. Christensen (1998), Mineral abundance determination: Quantitative deconvolution of thermal emission spectra, *J. Geophys. Res.*, *103*, 577–596, doi:10.1029/97JB02784.

Ramsey, M. S., and J. Dehn (2004), Spaceborne observations of the 2000 Bezymianny, Kamchatka eruption: The integration of high-resolution ASTER data into near real-time monitoring using AVHRR, *J. Volcanol. Geotherm. Res.*, *135*, 127–146, doi:10.1016/j.jvolgeores.2003.12.014.

Ramsey, M. S., and J. H. Fink (1999), Estimating silicic lava vesicularity with thermal remote sensing: A new technique for volcanic mapping and monitoring, *Bull. Volcanol.*, *61*, 32–39, doi:10.1007/s004450050260.

Realmuto, V. J., K. Hon, A. B. Kahle, E. A. Abbott, and D. C. Pieri (1992), Multispectral thermal infrared mapping of the 1 October 1988 Kupaianaha flow field, Kilauea Volcano, Hawaii, *Bull. Volcanol.*, *55*, 33–44, doi:10.1007/BF00301118.

Ruff, S. W., P. R. Christensen, P. W. Barbera, and D. L. Anderson (1997), Quantitative thermal emission spectroscopy of minerals: A laboratory technique for measurement and calibration, *J. Geophys. Res.*, *102*, 14,899–14,913, doi:10.1029/97JB00593.

Salisbury, J. W., and A. Wald (1992), The role of volume scattering in reducing spectral contrast of Reststrahlen bands in spectra of powdered minerals, *Icarus*, *96*, 121–128, doi:10.1016/0019-1035(92)90009-V.

Salisbury, J. W., L. S. Walter, N. Vergo, and D. M. D'Aria (1991), *Infrared (2.1–25 μm) Spectra of Minerals*, 267 pp., Johns Hopkins Univ. Press, Baltimore, Md.

Schairer, J. (1957), Melting relations of the common rock-forming oxides, *J. Am. Ceram. Soc.*, *40*, 215–235, doi:10.1111/j.1151-2916.1957.tb12608.x.

Stebbins, J. F. (1995), Dynamics and structure of silicate and oxide melts: Nuclear magnetic resonance studies, in *Structure, Dynamics and Properties of Silicate Melts*, *Rev. Mineral*, vol. 33, edited by J. F. Stebbins et al., pp. 191–246, Mineral. Soc. Am., Blacksburg, Va.

Sweet, J. R., and W. B. White (1969), Study of sodium silicate glasses and liquids by infrared reflectance spectroscopy, *Phys. Chem. Glasses*, *10*, 246–251.

Vaughan, R. G., R. Wessels, and M. S. Ramsey (2005), Monitoring renewed volcanic activity at Mount St. Helens with high-resolution thermal infrared data: ASTER, MASTER and FLIR, *Eos Trans. AGU*, *86*(52), Fall Meet. Suppl., Abstract V53D-1603.

Walter, L. S., and J. W. Salisbury (1989), Spectral characterization of igneous rocks in the 8 to 12 μm region, *J. Geophys. Res.*, *94*, 9203–9213, doi:10.1029/JB094iB07p09203.

Wright, S. P., and M. S. Ramsey (2006), Thermal infrared data analyses of Meteor Crater, Arizona: Implications for Mars spaceborne data from the Thermal Emission Imaging System, *J. Geophys. Res.*, *111*, E02004, doi:10.1029/2005JE002472.

Wyatt, M. B., V. E. Hamilton, H. Y. McSween Jr., and P. R. Christensen (2001), Analysis of terrestrial and Martian volcanic compositions using thermal emission spectroscopy: I. Determination of mineralogy, chemistry, and classification strategies, *J. Geophys. Res.*, *106*, 14,711–14,732, doi:10.1029/2000JE001356.

P. L. King, Institute of Meteoritics, University of New Mexico, Albuquerque, NM 87131, USA.

R. J. Lee and M. S. Ramsey, Department of Geology and Planetary Science, 200 SRCC Bldg., University of Pittsburgh, Pittsburgh, PA 15260, USA. (rjl20@pitt.edu)